J|A|C|S
ARTICLES

Published on Web 07/17/2009

Isolation of Dysprosium and Yttrium Complexes of a Three-Electron Reduction Product in the Activation of Dinitrogen, the $(N_2)^{3-}$ Radical

William J. Evans,*,† Ming Fang,† Gaël Zucchi,†,§ Filipp Furche,† Joseph W. Ziller,† Ryan M. Hoekstra,‡ and Jeffrey I. Zink‡

Department of Chemistry, University of California, Irvine, California 92697 and, Department of Chemistry and Biochemistry, University of California, Los Angeles, California 90095

Received May 12, 2009; E-mail: wevans@uci.edu

Abstract: DyI_2 reacts with 2 equiv of KOAr (OAr = $OC_6H_3(CMe_3)_2$-2,6) under nitrogen to form not only the $(N_2)^{2-}$ complex, $[(ArO)_2(THF)_2Dy]_2(\mu\text{-}\eta^2\text{:}\eta^2\text{-}N_2)$, **1**, but also complexes of similar formula with an added potassium ion, $[(ArO)_2(THF)Dy]_2(\mu\text{-}\eta^2\text{:}\eta^2\text{-}N_2)[K(THF)_6]$, **2**, and $[(ArO)_2(THF)Dy]_2(\mu_3\text{-}\eta^2\text{:}\eta^2\text{:}\eta^2\text{-}N_2)K(THF)$, **3**. The 1.396(7) and 1.402(7) Å N−N bond distances in **2** and **3**, respectively, are consistent with an $(N_2)^{3-}$ ligand, but the high magnetic moment of $4f^9$ Dy^{3+} precluded definitive identification. The $Y[N(SiMe_3)_2]_3$/K reduction system was used to synthesize yttrium analogues of **2** and **3**, $\{[(Me_3Si)_2N]_2(THF)Y\}_2(\mu\text{-}\eta^2\text{:}\eta^2\text{-}N_2)[K(THF)_6]$ and $\{[(Me_3Si)_2N]_2(THF)Y\}_2(\mu_3\text{-}\eta^2\text{:}\eta^2\text{:}\eta^2\text{-}N_2)K$, that had similar N−N distances and allowed full characterization. EPR, Raman, and DFT studies are all consistent with the presence of $(N_2)^{3-}$ in these complexes. ^{15}N analogues were also prepared to confirm the spectroscopic assignments. The DFT studies suggest that the unpaired electron is localized primarily in a dinitrogen π orbital isolated spatially, energetically, and by symmetry from the metal orbitals.

Introduction

Reproducing the biological transformation of dinitrogen to ammonia that occurs under ambient conditions in Nature has been one of the grand challenges to chemists for decades.[1−6] Although it was known since 1909 that dinitrogen can be reduced with hydrogen at high temperature and pressure via the Haber−Bosch process, a discovery that forms the basis of our modern fertilizer industry,[7] it has proven difficult to develop synthetic mimics of this multielectron reduction process that function under milder conditions. Major advances have been made in dinitrogen reduction in recent years including the development of a room temperature catalytic cycle.[1,8] Two main schemes, the Chatt and the Schrock cycles, have evolved to explain the sequence of reactions involved in biological dinitrogen reduction.[1−3] This paper describes metal complexes of a previously unobserved dinitrogen reduction product that has not been in these dinitrogen reduction schemes, namely the $(N_2)^{3-}$ radical, the result of a three-electron reduction of dinitrogen.

Most studies of dinitrogen reduction have been appropriately done with transition metals since these metals are involved in both the natural system and the Haber−Bosch process. However, studies with unusual metals, like the lanthanides and actinides, can be valuable in studying such multielectron processes in that these large, extremely electropositive metals can allow the isolation of unexpected species. For example, reduction of dinitrogen with the Sm^{2+} lanthanide metallocene, $(C_5Me_5)_2Sm$,[9] revealed the first bimetallic dinitrogen reduction product of any kind in which the M_2N_2 core was planar, i.e. $[(C_5Me_5)_2Sm]_2(\mu\text{-}\eta^2\text{:}\eta^2\text{-}N_2)$.[10] Although the coplanar M_2N_2 unit was subsequently identified in transition metal complexes,[11−16] it has proven to be prevalent in lanthanide chemistry where over 20 crystallographically characterized examples of general formula, $[Z_2(THF)_xLn]_2(\mu\text{-}\eta^2\text{:}\eta^2\text{-}N_2)]$ (Z = $(C_5Me_5)^{1-}$, $(C_5Me_4H)^{1-}$, $(C_5H_4SiMe_3)^{1-}$, $[N(SiMe_3)_2]^{1-}$, $[OC_6H_3(CMe_3)_2\text{-}2,6]^{1-}$; x =

† University of California, Irvine.
‡ University of California, Los Angeles.
§ Current address: CEA, IRAMIS, SIS2M, Laboratoire Claude Fréjacques, CNRS URA 331, 91191 Gif-sur-Yvette, France.

(1) Schrock, R. R. *Angew. Chem., Int. Ed.* **2008**, *47*, 5512–5522.
(2) Stephan, G. C.; Sivasankar, C.; Studt, F.; Tuczek, F. *Chem.—Eur. J.* **2008**, *14*, 644–652.
(3) Studt, F.; Tuczek, F. *J. Comput. Chem.* **2006**, *27*, 1278–1291.
(4) Fryzuk, M. D.; Johnson, S. A. *Coord. Chem. Rev.* **2000**, 200–202, 379–409.
(5) Schlögl, R. *Angew. Chem., Int. Ed.* **2003**, *42*, 2004–2008.
(6) Chirik, P. J. *Dalton Trans.* **2007**, 16–25.
(7) Smil, V. *Enriching the Earth: Fritz Haber, Carl Bosch, and the Transformation of World Food Production.*; MIT Press: Cambridge, 2004.
(8) Yandulov, D. V.; Schrock, R. R. *Science* **2003**, *301*, 76–78.
(9) Evans, W. J.; Hughes, L. A.; Hanusa, T. P. *J. Am. Chem. Soc.* **1984**, *106*, 4270–4272.
(10) Evans, W. J.; Ulibarri, T. A.; Ziller, J. W. *J. Am. Chem. Soc.* **1988**, *110*, 6877–6879.
(11) Fryzuk, M. D.; Love, J. B.; Rettig, S. J.; Young, V. G. *Science* **1997**, *275*, 1445–1447.
(12) Pool, J. A.; Lobkovsky, E.; Chirik, P. J. *Nature* **2004**, *427*, 527–530.
(13) Fryzuk, M. D. *Acc. Chem. Res.* **2009**, *42*, 127–133.
(14) Pool, J. A.; Chirik, P. J. *Can. J. Chem.* **2005**, *83*, 286–295.
(15) Bernskoetter, W. H.; Pool, J. A.; Lobkovsky, E.; Chirik, P. J. *J. Am. Chem. Soc.* **2005**, *127*, 7901–7911.
(16) MacLachlan, E. A.; Fryzuk, M. D. *Organometallics* **2006**, *25*, 1530–1543.

0−2) are now known.[17−24] These $Ln_2(\mu\text{-}\eta^2\text{:}\eta^2\text{-}N_2)$ complexes were made initially with reactive divalent lanthanide ions such as Sm^{2+},[10] Tm^{2+},[20] Dy^{2+},[21] and Nd^{2+},[22] eq 1. However, subsequently it was found that combinations of salts of

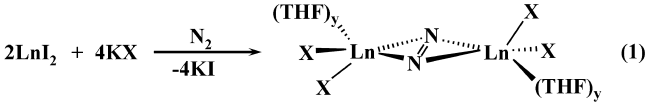

(1)

Ln = Sm, Tm, Dy, Nd
X = $N(SiMe_3)_2$, $OC_6H_3(CMe_3)_2$-2,6, C_5Me_5, $C_5H_4SiMe_3$; y = 0-2

trivalent lanthanide ions, Ln^{3+}, in the presence of alkali metals can provide planar Ln_2N_2 complexes via analogous Ln^{2+}-like reactivity even if the divalent ion was not isolable, eq 2.[23,24] These $Ln_2(\mu\text{-}\eta^2\text{:}\eta^2\text{-}N_2)$ complexes typically have N−N distances between 1.233(5) and 1.285(4) Å and are well

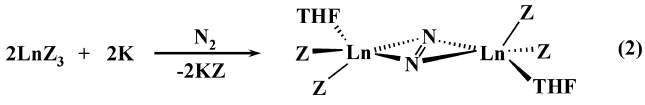

(2)

Ln = La, Ce, Pr, Nd, Gd, Tb, Dy, Ho, Er, Y, Tm, Lu
Z = $N(SiMe_3)_2$, C_5Me_4H

represented as products of a two-electron reduction of the triple bond in N_2 to a double bond, i.e. $(N{=}N)^{2-}$.

When dinitrogen reduction according to eq 1 was studied with Dy^{2+} and Z = $OC_6H_3(CMe_3)_2$-2,6, a new type of reduced dinitrogen complex was identified that was very similar to the $(N_2)^{2-}$ compounds discussed above except that an alkali metal cation was also present. Charge balance required that the dinitrogen unit located between the metals carry a 3− charge. This suggested the presence of a $(N_2)^{3-}$ radical, a species previously unobserved in dinitrogen reduction chemistry to our knowledge. However, an alternative possibility was a protonated version of the known $(N_2)^{4-}$ ion,[12,25−31] i.e., $(N_2H)^{3-}$.[32] Complexes of *di*protonated $(N_2)^{4-}$ ions, i.e., $(N_2H_2)^{2-}$ compounds, are well-known.[27] By expanding the studies of the paramagnetic Dy^{3+} complexes to analogues of chemically similar Y^{3+}, which is diamagnetic, definitive evidence on the reduced dinitrogen species was obtained as reported here.

Experimental Section

The syntheses and manipulations described below were conducted under argon or nitrogen with rigorous exclusion of air and water using glovebox, vacuum line, and Schlenk techniques. $AgBPh_4$ and AgOTf were purchased from Aldrich and used as received. Potassium was purchased from Aldrich, washed with hexanes, and scraped to provide shiny pieces before use. Potassium graphite[33] and $Y[N(SiMe_3)_2]_3$[34] were prepared according to literature methods. Potassium 2,6-di-*tert*-butylphenoxide was synthesized from potassium hydride and 2,6-di-*tert*-butylphenol in THF. DyI_2 was synthesized by a solid phase reaction between dysprosium metal and iodine.[35] Solvents were dried over columns containing Q-5 and molecular sieves. NMR solvents were dried over sodium−potassium alloy, degassed, and vacuum transferred prior to use. ^1H and ^{13}C NMR spectra were obtained on a Bruker DRX500 MHz spectrometer at 25 °C. IR samples were prepared as KBr pellets, and the spectra were obtained on a Varian 1000 FT-IR system. Elemental analyses were performed by Analytische Laboratorien (Lindlar, Germany). Electron paramagnetic resonance spectra were collected using a Bruker EMX spectrometer equipped with an ER041XG microwave bridge. The magnetic field was calibrated with DPPH, and all experiments were done at room temperature. SIMPOW6[36] developed by Professor Nilges at University of Illinois was used to simulate the EPR spectra. Raman spectra were recorded using a Jobin-Yvon HR 640 triple monochromator equipped with a CCD detector (Roper Scientific Model 7375-0001) operating at −120 °C. A Coherent I-300C krypton ion laser operating between 5 and 25 mW was used as the excitation source. The sample (∼10 mg) was sealed in a quartz EPR tube (4 mm OD) and chilled nitrogen was blown on the sample, obtaining temperatures of 5 to 10 °C while irradiating. Compound **4** is most resonantly enhanced in the near-UV to UV when KNO_3 is used as an internal standard. Compound **6** was observed by exciting at 530.9 nm, although the resonant maxima of the compound cannot be determined.

$[(ArO)_2(THF)_2Dy]_2(\mu\text{-}\eta^2\text{:}\eta^2\text{-}N_2)$], 1; $[(ArO)_2(THF)Dy]_2(\mu\text{-}\eta^2\text{:}\eta^2\text{-}N_2)[K(THF)_6]$, 2; and $[(ArO)_2(THF)Dy]_2(\mu_3\text{-}\eta^2\text{:}\eta^2\text{:}\eta^2\text{-}N_2)K(THF)$, 3. In an argon-filled glovebox, a 50 mL round-bottom flask was charged with potassium 2,6-di-*tert*-butylphenoxide (500 mg, 2.05 mmol) and DyI_2 (341 mg, 0.82 mmol). The flask was connected to a high-vacuum line, and ∼30 mL of THF were transferred under vacuum. N_2 (1 atm) was introduced into the flask while the solvent was frozen, and the mixture was allowed to warm to −78 °C with stirring. A dark purple solution initially formed, which slowly turned dark brown. After 2 h, the brown solution was allowed to warm to RT and stirred for an additional 1 h. The solvent was evaporated under vacuum, and the residue was extracted with 10 mL of hexane, concentrated, and stored at −35 °C. Complex **3** (28 mg, 0.02 mmol, 4%) was obtained from the hexane extract in 2 d as brown crystals. The hexane insoluble reaction products were extracted with 5 mL of THF, and the extract was centrifuged. From the dark brown-reddish solution, brown crystals of **2**·2THF (161 mg, 0.09 mmol, 20%) and yellow crystals of **1**·4THF (20 mg, 0.014 mmol, 3%) were isolated at −35 °C. Anal. Calcd for $Dy_2C_{96}H_{164}N_2O_{14}K$, **2**·2THF: C, 59.61; H, 8.55; N, 1.45; K, 2.02; Dy, 16.80. Found:

(17) Evans, W. J.; Lee, D. S. *Can. J. Chem.* **2005**, *83*, 375–384.
(18) Dubé, T.; Ganesan, M.; Conoci, S.; Gambarotta, S.; Yap, G. P. A. *Organometallics* **2000**, *19*, 3716–3721.
(19) Jaroschik, F.; Momin, A.; Nief, F.; Goff, X. L.; Deacon, G. B.; Junk, P. C. *Angew. Chem., Int. Ed.* **2009**, *48*, 1117–1121.
(20) Evans, W. J.; Allen, N. T.; Ziller, J. W. *J. Am. Chem. Soc.* **2001**, *123*, 7927–7928.
(21) Evans, W. J.; Allen, N. T.; Ziller, J. W. *Angew. Chem., Int. Ed.* **2002**, *41*, 359–361.
(22) Evans, W. J.; Zucchi, G.; Ziller, J. W. *J. Am. Chem. Soc.* **2003**, *125*, 10–11.
(23) Evans, W. J.; Lee, D. S.; Rego, D. B.; Perotti, J. M.; Kozimor, S. A.; Moore, E. K.; Ziller, J. W. *J. Am. Chem. Soc.* **2004**, *126*, 14574–14582.
(24) Evans, W. J.; Lee, D. S.; Lie, C.; Ziller, J. W. *Angew. Chem., Int. Ed.* **2004**, *43*, 5517–5519.
(25) Hirotsu, M.; Fontaine, P. P.; Zavalij, P. Y.; Sita, L. R. *J. Am. Chem. Soc.* **2007**, *129*, 12690–12692.
(26) MacLachlan, E. A.; Hess, F. M.; Patrick, B. O.; Fryzuk, M. D. *J. Am. Chem. Soc.* **2007**, *129*, 10895–10905.
(27) Bernskoetter, W. H.; Olmos, A. V.; Lobkovsky, E.; Chirik, P. J. *Organometallics* **2006**, *25*, 1021–1027.
(28) Dubé, T.; Conoci, S.; Gambarotta, S.; Yap, G. P. A.; Vasapollo, G. *Angew. Chem., Int. Ed.* **1999**, *38*, 3657–3659.
(29) Bérubé, C. D.; Yazdanbakhsh, M.; Gambarotta, S.; Yap, G. P. A. *Organometallics* **2003**, *22*, 3742–3747.
(30) Guillemot, G.; Castellano, B.; Prangé, T.; Solari, E.; Floriani, C. *Inorg. Chem.* **2007**, *46*, 5152–5154.
(31) Jubb, J.; Gambarotta, S. *J. Am. Chem. Soc.* **1994**, *116*, 4477–4478.
(32) Basch, H.; Musaev, D. G.; Morokuma, K.; Fryzuk, M. D.; Love, J. B.; Seidel, W. W.; Albinati, A.; Koetzle, T. F.; Klooster, W. T.; Mason, S. A.; Eckert, J. *J. Am. Chem. Soc.* **1999**, *121*, 523–528.
(33) Bergbreiter, D. E.; Killough, J. M. *J. Am. Chem. Soc.* **1978**, *100*, 2126–2134.
(34) Edelmann, F. T.; Poremba, P. In *Synth. Methods Organomet. Inorg. Chem.*; Herrmann, W. A., Ed.; Thieme Verlag: Stuttgart, 1997; Vol. 6, pp 37–40.
(35) Evans, W. J.; Allen, N. T.; Workman, P. S.; Meyer, J. C. *Inorg. Chem.* **2003**, *42*, 3097–3099.
(36) Nilges, M. J.; Mattson, K. J.; Belford, R. L. In *ESR Spectroscopy in Membrane Biophysics, Biological Magnetic Resonance*; Hemminga, M. A., Berliner, L., Eds.; Springer: New York, 2006; Vol. 27, pp 261–281.

Table 1. X-ray Data Collection Parameters

	$C_{72}H_{116}Dy_2N_2O_8 \cdot 4(C_4H_8O)$ **1** · 4THF	$C_{72}H_{116}Dy_2N_2O_8 \cdot 2(C_7H_8)$ **1** · 2toluene	$C_{88}H_{148}Dy_2KN_2O_{12} \cdot 2(C_4H_8O)$ **2** · 2THF	$C_{68}H_{108}Dy_2KN_2O_7 \cdot C_6H_{14}$ **3** · hexane	$C_{56}H_{136}KN_6O_8Si_8Y_2$ **5**	$C_{32}H_{88}KN_6O_2Si_8Y_2 \cdot {}^1/_2(C_7H_8)$ **6** · $^1/_2$toluene
formula weight	1751.08	1646.94	1934.39	1515.84	1463.35	1076.79
T (K)	168(2)	178(2)	138(2)	138(2)	153(2)	103(2)
crystal system	triclinic	monoclinic	triclinic	triclinic	monoclinic	monoclinic
space group	$P\bar{1}$	$P2_1/c$	$P\bar{1}$	$P\bar{1}$	$P2_1/n$	$P2_1/n$
A (Å)	12.2397(6)	15.5427(5)	12.8686(6)	14.0906(9)	16.4627(9)	12.481(3)
B (Å)	12.8327(6)	12.0654(4)	13.3829(6)	18.0226(12)	24.9416(13)	21.371(5)
C (Å)	15.0834(7)	24.6783(8)	16.2559(7)	19.2315(13)	19.9471(11)	22.304(5)
α (deg)	74.2110(10)	90	109.2667(7)	68.0610(11)	90	90
β (deg)	82.3250(10)	105.2250(10)	99.9592(8)	85.6165(11)	93.6840(10)	105.071(3)
γ (deg)	73.6930(10)	90	104.5794(8)	68.4163(11)	90	90
volume (Å^3)	2183.83(18)	4465.5(3)	2455.21(19)	4201.9(5)	8173.5(8)	5744(2)
Z	1	2	1	2	4	4
ρ_{calcd} (Mg/m^3)	1.331	1.225	1.308	1.198	1.189	1.245
μ (mm^{-1})	1.755	1.710	1.611	1.858	1.627	2.282
R1 [$I > 2.0\sigma(I)$]	0.0441	0.0494	0.0369	0.0532	0.0567	0.0372
wR2 (all data)	0.1131	0.1664	0.0948	0.1616	0.1706	0.0910

C, 59.31; H, 8.29; N, 1.61; K, 2.10; Dy, 16.96. $\mu_{eff} = 9.8\ \mu_B$. Anal. Calcd for $Dy_2C_{68}H_{108}KN_2O_7$, **3**: Dy, 22.7. Found: Dy, 22.2.

[(ArO)$_2$(THF)$_2$Dy]$_2$(μ-η^2:η^2-N$_2$), 1. In an argon-filled glovebox, a solution of **2**·2THF (65 mg, 0.034 mmol) in 5 mL of THF was added at ambient temperature to a solution of $AgBPh_4$ (20 mg, 0.047 mmol) in 15 mL of THF in a vial covered with aluminum foil. After stirring for 2 h, the mixture was centrifuged to eliminate a black precipitate (Ag). The yellow solution was evaporated, and the residue was extracted with 2 mL of toluene. The mixture was centrifuged to eliminate a white solid ($KBPh_4$), and 1 mL of hexane was added. Crystals of **1** (13 mg, 0.009 mmol, 26%) were obtained after 2 d at −35 °C. Anal. Calcd for $Dy_2C_{72}H_{116}N_2O_8$·toluene: C, 61.03; H, 8.04; N, 1.80; Dy, 20.90. Found: C, 60.64; H, 7.81; N, 1.96; Dy, 21.17. $\mu = 10.0\ \mu_B$.

{[(Me$_3$Si)$_2$N]$_2$(THF)Y}$_2$(μ-η^2:η^2-N$_2$)[K(THF)$_6$], 5, and {[(Me$_3$Si)$_2$N]$_2$(THF)Y}$_2$(μ_3-η^2:η^2:η^2-N$_2$)K, 6. In a nitrogen-filled glovebox, potassium graphite (0.760 g, 5.62 mmol) was slowly added at ambient temperature to a stirred solution of $Y[N(SiMe_3)_2]_3$ (3.20 g, 5.62 mmol) in 40 mL of THF over 20 min. The solution immediately became orange and was allowed to stir for an additional 30 min. The reaction mixture was centrifuged and filtered to remove dark insoluble material and evaporation of the filtrate yielded a yellow tacky solid. The yellow solid was dissolved in 5 mL of THF and stored at −35 °C for 2 d to produce complex **5** (0.81 g, 0.56 mmol, 20%) as orange crystals. Complex **6** was produced as yellow crystals at −35 °C over 2−3 d when toluene was used for recrystallization. Anal. Calcd for $Y_2C_{32}H_{88}N_6O_2Si_8K$, **6**: C, 37.29; H, 8.61; N, 8.15; Si, 21.80; K, 3.79; Y, 17.25. Found: C, 36.92; H, 8.47; N, 7.45; Si, 20.94; K, 4.06; Y, 19.86. IR: 2947m, 2893m, 1437w, 1245s, 1018m, 979s, 868s, 828s, 771m, 751m, 665m, 608m cm^{-1}.

{[(Me$_3$Si)$_2$N]$_2$(THF)Y}$_2$(μ-η^2:η^2-N$_2$), 4. In a nitrogen-filled glovebox, AgOTf (12 mg, 0.048 mmol) was added at ambient temperature to a solution of **5** (71 mg, 0.048 mmol) in 5 mL of THF. The mixture immediately turned black. After stirring for 20 min, the mixture was centrifuged to eliminate a black precipitate (Ag). The brown solution was evaporated, and the residue was extracted with 2 mL of hexane. The mixture was centrifuged and filtered. Complex **4** (30 mg, 0.030 mmol, 62%) was obtained as a pale blue solid after evaporation of the supernatant.

X-ray Data Collection, Structure Solution, and Refinement. For all the structures, the APEX[37] or SMART[38] program package was used to determine the unit-cell parameters and for data collection (25 s/frame scan time for a sphere of diffraction data for compounds **1**·2toluene, **3**, and **6**; 30 s/frame scan time for compounds **1**·4THF, **2**, and **5**). The raw frame data were processed using SAINT[39] and SADABS[40] to yield the reflection data file. Subsequent calculations were carried out using the SHELXTL[41] program. Details are given in Table 1.

Computational Details. The structures of **4**, **5**, and **6** were initially optimized using the TPSSH[42] hybrid meta-GGA functional and split valence basis sets with polarization functions on non-hydrogen atoms (SV(P)).[43] TPSSH was chosen due to its established performance for transition metal compounds;[44,45] the 10% fraction of exact exchange reduces the self-interaction error in the results for the radical anion **5**. Relativistic small-core pseudopotentials[46] were employed for Y. Fine quadrature grids (size m4)[47] were used throughout. Vibrational frequencies were computed at the TPSSH/SV(P) level[48] and scaled by a factor of 0.95 to account for anharmonicity and basis set incompleteness; this factor was chosen to approximately fit the computed vibrational frequency of free N_2 to the gas phase value[49] of 2359 cm^{-1}. All structures were found to be minima. Natural population analyses[50] and plots were also obtained at the TPSSH/SV(P) level; the contour values were 0.06 for molecular orbital plots and 0.005 for the spin density plot. The

(37) *APEX2*, version 2.2−0; Bruker AXS, Inc.: Madison, WI, 2007. *APEX2*, version 2008.3-0; Bruker AXS, Inc.: Madison, WI, 2008.
(38) *SMART Software Users Guide*, version 5.1; Bruker Analytical X-Ray Systems, Inc.: Madison, WI, 1999.
(39) *SAINT Software Users Guide*, version 6.0; Bruker AXS, Inc.: Madison, WI, 1999. *SAINT*, version 7.46a; Bruker AXS, Inc.: Madison, WI, 2007. *SAINT*, version 7.53a; Bruker AXS, Inc.: Madison, WI, 2007.
(40) Sheldrick, G. M. *SADABS*, version 2.03; Bruker AXS, Inc.: Madison, WI, 2000. Sheldrick, G. M. *SADABS*, version 2008/1; Bruker AXS, Inc.: Madison, WI, 2008.
(41) Sheldrick, G. M. *SHELXTL*, version 6.12; Bruker AXS, Inc.: Madison, WI, 2001.
(42) Staroverov, V. N.; Scuseria, G. E.; Tao, J.; Perdew, J. P. *J. Chem. Phys.* **2003**, *119*, 12129–12137.
(43) Schäfer, A.; Horn, H.; Ahlrichs, R. *J. Chem. Phys.* **1992**, *97*, 2571–2577.
(44) Furche, F.; Perdew, J. P. *J. Chem. Phys.* **2006**, *124*, 044103(1)−044103(27) .
(45) Waller, M. P.; Braun, H.; Hojdis, N.; Buhl, M. *J. Chem. Theory Comput.* **2007**, *3*, 2234–2242.
(46) Andrae, D.; Haussermann, U.; Dolg, M. *Theor. Chim. Acta* **1990**, *77*, 123–141.
(47) Treutler, O.; Ahlrichs, R. *J. Chem. Phys.* **1995**, *102*, 346–354.
(48) Deglmann, P.; Furche, F.; Ahlrichs, R. *Chem. Phys. Lett.* **2002**, *362*, 511–518.

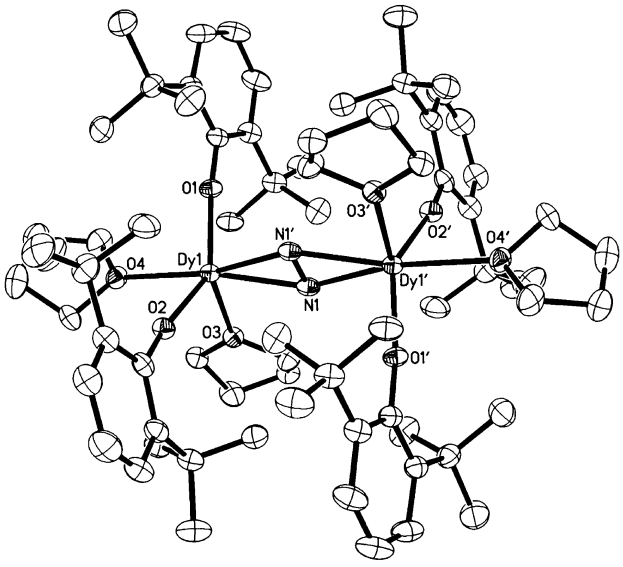

Figure 1. Thermal ellipsoid plot of $[(ArO)_2(THF)_2Dy]_2(\mu\text{-}\eta^2\text{:}\eta^2\text{-}N_2)$, **1**, $(OAr = OC_6H_3(CMe_3)_2\text{-}2,6)$ drawn at the 50% probability level. Hydrogen atoms have been omitted for clarity.

structural parameters reported in the text are the result of reoptimization using larger triple-ζ valence basis sets with two sets of polarization functions (def2-TZVP).[51] The differences between the SV(P) and the TZVP structures were found to be small, typically amounting to 0.01 Å in bond lengths or less. All computations were performed using the TURBOMOLE program package.[52]

Results and Discussion

The reaction of divalent DyI_2 with 2 equiv of KOAr $(OAr = OC_6H_3(CMe_3)_2\text{-}2,6)$ at −78 °C under N_2 in THF does not simply give the $[(ArO)_2(THF)_2Dy]_2(\mu\text{-}\eta^2\text{:}\eta^2\text{-}N_2)$ product, **1**, Figure 1, analogous to the $[Z_2(THF)_xLn]_2(\mu\text{-}\eta^2\text{:}\eta^2\text{-}N_2)$ complexes previously isolated according to eq 1.[22] Instead, as shown in Scheme 1, it affords a mixture of products that contains more of the potassium salt, $[(ArO)_2(THF)Dy]_2(\mu\text{-}\eta^2\text{:}\eta^2\text{-}N_2)[K(THF)_6]$, **2**, Figure 2, than complex **1** and a small amount of $[(ArO)_2(THF)\text{-}Dy]_2(\mu_3\text{-}\eta^2\text{:}\eta^2\text{:}\eta^2\text{-}N_2)K(THF)$, **3**, Figure 3. Complexes **2** and **3** can be interconverted by removal and addition of THF, Scheme 1.

X-ray crystallography showed that complexes **1**−**3** each had a Dy_2N_2 core but that the N−N bond lengths differed (Table 2). The 1.257(7) Å N−N distance in **1** was similar to the 1.233(5)−1.285(4) Å N−N distances observed in all the other Ln_2N_2 complexes made via eqs 1 and 2 containing $(N{=}N)^{2-}$ ligands.[17,19−24] The N−N distances in **2** and **3**, 1.396(7) and 1.402(7) Å, respectively, were longer and are in between the range for N=N double bonds, e.g., 1.25 Å in PhN=NPh, and N−N single bonds, e.g., 1.47 Å in H_2NNH_2.[53] Comparisons of these distances in **2** and **3** with those in $(N_2)^{4-}$ complexes in the literature are more complicated since these range from 1.377(2) to 1.635(5) Å.[12,25−31] The fact that the N−N distances in **2** and **3** were intermediate between a single and double N−N bond could be consistent with the presence of a $(N_2)^{3-}$ radical

Scheme 1. Reactivity of Dinitrogen with the Dysprosium Reduction System, DyI_2/2KOAr $(OAr = OC_6H_3(CMe_3)_2\text{-}2,6)$

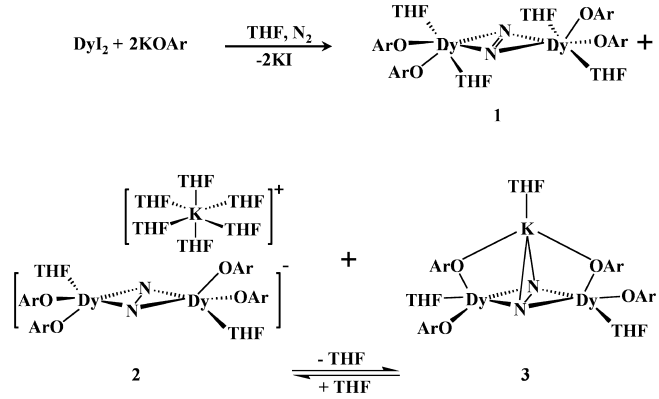

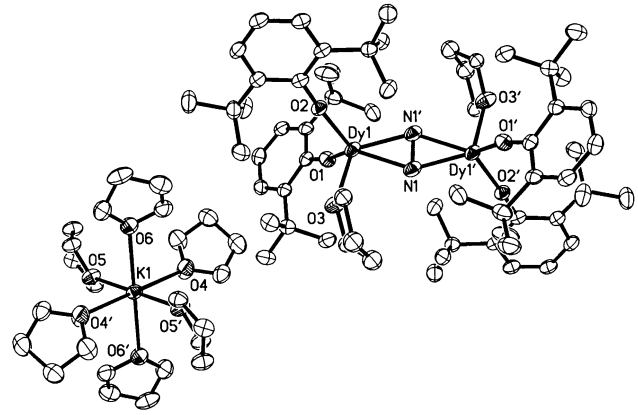

Figure 2. Thermal ellipsoid plot of $[(ArO)_2(THF)Dy]_2(\mu\text{-}\eta^2\text{:}\eta^2\text{-}N_2)[K(THF)_6]$, **2**, drawn at the 50% probability level. Hydrogen atoms have been omitted for clarity.

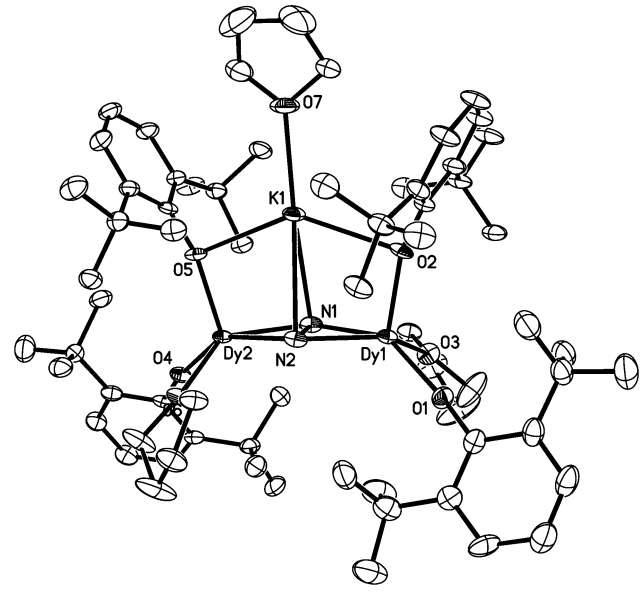

Figure 3. Thermal ellipsoid plot of $[(ArO)_2(THF)Dy]_2(\mu_3\text{-}\eta^2\text{:}\eta^2\text{:}\eta^2\text{-}N_2)K(THF)$, **3**, drawn at the 50% probability level. Hydrogen atoms have been omitted for clarity.

(49) Huber, K. P.; Herzberg, G. *Constants of Diatomic Molecules (data prepared by Gallagher, J. W. & Johnson, R. D. III) in NIST Chemistry WebBook, NIST Standard Reference Database Number 69*; Linstrom, P. J., Mallard, W. G., Eds.; National Institute of Standards and Technology: Gaithersburg, MD, 20899. http://webbook.nist.gov (retrieved February 23, 2009).
(50) Reed, A. E.; Weinstock, R. B.; Weinhold, F. *J. Chem. Phys.* **1985**, *83*, 735–746.
(51) Weigend, F.; Ahlrichs, R. *Phys. Chem. Chem. Phys.* **2005**, *18*, 3297–3305.
(52) *TURBOMOLE*, V6-0; TURBOMOLE GmbH: Karlsruhe, 2008. http://www.turbomole.com.
(53) Allen, N. T.; Kennard, O.; Watson, D. G.; Brammer, L.; Orpen, A. G.; Taylor, R. *J. Chem. Soc., Perkin Trans. 2* **1987**, S1−S19.

Table 2. Selected Bond Lengths (Å) and Angles (deg) in $[(ArO)_2(THF)_2Dy]_2(\mu\text{-}\eta^2\text{:}\eta^2\text{-}N_2)\cdot 4C_4H_8O$, **1**·4THF; $[(ArO)_2(THF)_2Dy]_2(\mu\text{-}\eta^2\text{:}\eta^2\text{-}N_2)\cdot 2C_7H_8$, **1**·2Toluene; $[(ArO)_2(THF)Dy]_2(\mu\text{-}\eta^2\text{:}\eta^2\text{-}N_2)[K(THF)_6]$, **2**; $[(ArO)_2(THF)Dy]_2(\mu_3\text{-}\eta^2\text{:}\eta^2\text{:}\eta^2\text{-}N_2)K(THF)$, **3**; $\{[(Me_3Si)_2N]_2(THF)Y\}_2(\mu\text{-}\eta^2\text{:}\eta^2\text{-}N_2)$, **4**; $\{[(Me_3Si)_2N]_2(THF)Y\}_2(\mu\text{-}\eta^2\text{:}\eta^2\text{-}N_2)[K(THF)_6]$, **5**; and $\{[(Me_3Si)_2N]_2(THF)Y\}_2(\mu_3\text{-}\eta^2\text{:}\eta^2\text{:}\eta^2\text{-}N_2)K$, **6**

1·4THF		**1**·2Toluene	
N(1)−N(1′)	1.257(7)	N(1)−N(1′)	1.256(9)
Dy(1)−O(1)	2.161(3)	Dy(1)−O(1)	2.154(4)
Dy(1)−O(2)	2.163(3)	Dy(1)−O(2)	2.156(4)
Dy(1)−N(1)	2.328(4)	Dy(1)−N(1)	2.336(5)
Dy(1)−N(1′)	2.340(4)	Dy(1)−N(1′)	2.336(5)
Dy(1)−O(3)	2.413(3)	Dy(1)−O(3)	2.417(4)
Dy(1)−O(4)	2.499(3)	Dy(1)−O(4)	2.491(4)
N(1)−Dy(1)−N(1′)	31.24(17)	N(1)−Dy(1)−N(1′)	31.2(2)
Dy(1)−N(1)−Dy(1′)	148.76(17)	Dy(1)−N(1)−Dy(1′)	148.8(2)

2		**3**	
N(1)−N(1′)	1.396(7)	N(1)−N(2)	1.402(7)
Dy(1)−O(1)	2.154(2)	Dy(1)−O(1)	2.160(4)
Dy(1)−O(2)	2.158(2)	Dy(1)−O(2)	2.151(4)
Dy(1)−O(3)	2.434(3)	Dy(1)−O(3)	2.390(4)
Dy(1)−N(1)	2.197(3)	Dy(1)−N(1)	2.235(5)
Dy(1)-N(1′)	2.203(4)	Dy(1)−N(2)	2.209(5)
K(1)−O(4)	2.668(3)	Dy(2)−O(4)	2.168(4)
K(1)−O(5)	2.692(3)	Dy(2)−O(5)	2.148(4)
K(1)−O(6)	2.668(3)	Dy(2)−O(6)	2.398(4)
Dy(1)−N(1)−Dy(2)	143.01(17)	Dy(2)−N(1)	2.220(5)
N(1)−Dy(1)−N(1′)	37.00(17)	Dy(2)−N(2)	2.234(5)
		K(1)−O(2)	2.768(5)
		K(1)−O(5)	2.748(4)
		K(1)−O(7)	2.609(5)
		K(1)−N(1)	2.984
		K(1)−N(2)	3.003
		Dy(1)−N(1)−Dy(2)	142.2(2)
		Dy(1)−N(2)−Dy(2)	143.2(2)
		N(1)−Dy(1)−N(2)	36.78(18)
		N(1)−Dy(2)−N(2)	36.70(17)

4		**5**	
N(3)−N(3′)	1.268(3)	N(1)−N(1′)	1.401(6)
Y(1)−N(1)	2.2443(15)	Y(1)−N(2)	2.341(3)
Y(1)−N(2)	2.2640(15)	Y(1)−N(3)	2.303(3)
Y(1)−O(1)	2.3898(14)	Y(1)−O(1)	2.425(3)
Y(1)−N(3)	2.2958(17)	Y(1)−N(1)	2.194(3)
Y(1)−N(3′)	2.3170(16)	Y(1)−N(1′)	2.218(3)
N(3)−Y(1)−N(3′)	31.90(8)	K(1)−O(3)	2.545(8)
Y(1)−N(3)−Y(1′)	148.10(8)	K(1)−O(4)	2.653(8)
		K(1)−O(5)	2.678(5)
		K(1)−O(6)	2.692(4)
		K(1)−O(7)	2.711(4)
		K(1)−O(8)	2.685(4)
		N(1)−Y(1)−N(1′)	37.02(15)
		Y(1)−N(1)−Y(1′)	142.99(15)

6	
N(5)−N(6)	1.405(3)
Y(1)−N(1)	2.328(2)
Y(1)−N(2)	2.341(2)
Y(1)−O(1)	2.384(2)
Y(1)−N(5)	2.225(2)
Y(1)−N(6)	2.242(2)
Y(2)−N(3)	2.331(2)
Y(2)−N(4)	2.329(2)
Y(2)−O(2)	2.419(2)
Y(2)−N(5)	2.247(2)
Y(2)−N(6)	2.231(2)
K(1)−N(5)	2.864(2)
K(1)−N(6)	2.885(2)
K(1)−N(2)	2.982(3)
K(1)−N(4)	2.989(3)
Y(1)−N(5)−Y(2)	140.85(12)
Y(1)−N(6)−Y(2)	140.76(11)
N(5)−Y(1)−N(6)	36.67(9)

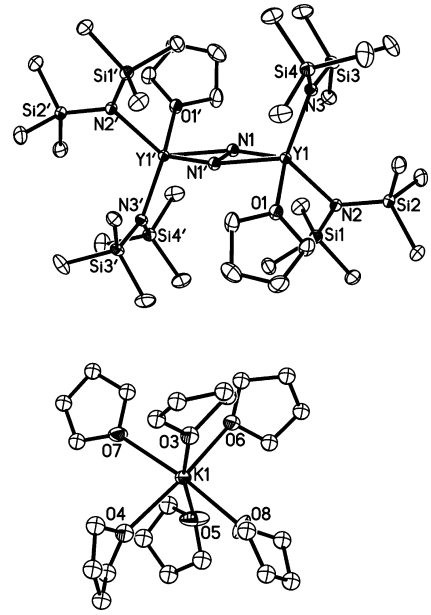

Figure 4. Thermal ellipsoid plot of $\{[(Me_3Si)_2N]_2(THF)Y\}_2(\mu\text{-}\eta^2\text{:}\eta^2\text{-}N_2)[K(THF)_6]$, **5**, drawn at the 30% probability level. Hydrogen atoms have been omitted for clarity.

with a formal bond order of 1.5. X-ray crystallographic studies of the isoelectronic superoxide anion, $(O_2)^{1-}$, show an analogous intermediate O−O bond distance, 1.28(2) Å[54] vs 1.21 Å for O_2 and 1.49 Å for $(O_2)^{2-}$.[55]

The lack of an N−H stretch in the infrared spectrum of **2** and no evidence of hydrogen when **2** was oxidized to **1** with $AgBPh_4$ supported the assignment of the $(N_2)^{3-}$ ligand shown in Scheme 1 rather than $(N_2H)^{3-}$. However, this negative evidence was not sufficient to claim the first example of a $(N_2)^{3-}$ ligand. EPR spectroscopy would normally be ideal to identify such a radical, but the data were complicated by the presence of the two paramagnetic $4f^9$ Dy^{3+} ions with magnetic moments of 9.8−10 μ_B.

To distinguish $(N_2)^{3-}$ from $(N_2H)^{3-}$, the synthesis of the analogous Y^{3+} complex was sought. Y^{3+} is a $4d^0$ ion close in size to Ho^{3+} that has chemistry similar to that of Dy^{3+} and other late lanthanides. Since yttrium has a 100% naturally abundant $I = {}^1/_2$ nucleus, analogous yttrium complexes could provide more information on the putative $(N_2)^{3-}$ species. Unfortunately, since Y^{2+} has never been observed in solution, a starting material analogous to the Dy^{2+} precursor, DyI_2, was not available. Furthermore, attempts to access Y^{2+}-like reactivity via LnZ_3/M methods,[23,24] eq 2, were unsuccessful with Ln = Y and Z = OAr. Hence, the desired combination of metal, ligand, and reductive method was not available to differentiate $(N_2)^{3-}$ from $(N_2H)^{3-}$.

To resolve this dilemma, the $Y[N(SiMe_3)_2]_3$/K system that previously generated the $(N_2)^{2-}$ product, $\{[(Me_3Si)_2N]_2(THF)Y\}_2(\mu\text{-}\eta^2\text{:}\eta^2\text{-}N_2)$, **4**,[23] according to eq 2, was examined further. It was found that variations in the method and rate of addition of potassium graphite to $Y[N(SiMe_3)_2]_3$ led to mixtures of products that contained orange products as well as the pale blue **4**. From these reactions, an yttrium amide analogue of **2**, namely $\{[(Me_3Si)_2N]_2(THF)Y\}_2(\mu\text{-}\eta^2\text{:}\eta^2\text{-}N_2)[K(THF)_6]$, **5**, Figure 4, was isolated. Removal of THF from **5** generated an yttrium amide analogue of

(54) Abrahams, S. C.; Kalnajs, J. *Acta Crystallogr.* **1955**, *8*, 503–506.
(55) Vaska, L. *Acc. Chem. Res.* **1976**, *9*, 175–183.

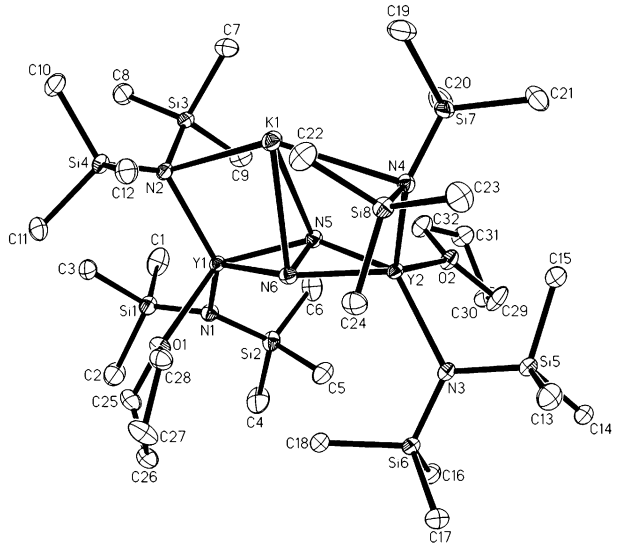

Figure 5. Thermal ellipsoid plot of $\{[(Me_3Si)_2N]_2(THF)Y\}_2(\mu_3\text{-}\eta^2\text{:}\eta^2\text{:}\eta^2\text{-}N_2)K$, **6**, drawn at the 30% probability level. Hydrogen atoms have been omitted for clarity.

3, namely $\{[(Me_3Si)_2N]_2(THF)Y\}_2(\mu_3\text{-}\eta^2\text{:}\eta^2\text{:}\eta^2\text{-}N_2)K$, **6**, Figure 5. Hence, as shown in Scheme 2, the $Y[N(SiMe_3)_2]_3/K$ system gives a mixture of products like that found with DyI_2 and KOAr, Scheme 1. Complexes **5** and **6** have 1.401(6) and 1.405(3) Å N−N distances, respectively, that are similar to those of **2** and **3** and longer than the 1.268(3) Å distance in **4**. Compounds **5** and **6** are also analogous to **2** and **3** in that they lack N−H absorptions in the infrared spectrum and **5** can be oxidized with AgOTf to **4**, eq 3.

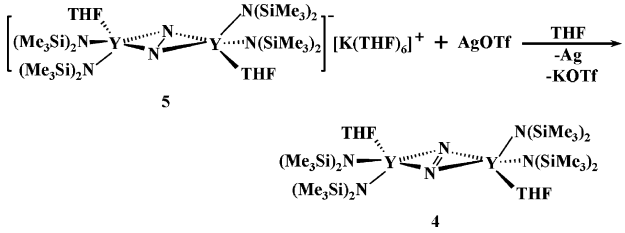

5

4 (3)

In contrast to **2** and **3**, definitive EPR spectra were obtainable with the yttrium complexes, **5** and **6**. The EPR spectrum of **5**, Figure 6a, contains a signal at $g = 2.0038$ that has a multiline pattern due to splitting by two ^{14}N ($I = 1$) and two ^{89}Y ($I = {}^1/_2$) nuclei. To simplify the spectrum and aid in simulation studies, the ^{15}N ($I = {}^1/_2$) analogue of **5** was synthesized from $^{15}N_2$. The 9-line pattern for **5-^{15}N** in Figure 6b is consistent with a triplet of triplets due to the splitting by two ^{15}N and two ^{89}Y nuclei. The simulations of **5** and **5-^{15}N** are also shown in Figure 6c and provide the hyperfine coupling constants of 3.1 G for ^{89}Y, 5.8 G for ^{14}N, and 8.2 G for ^{15}N, respectively. The EPR spectra of **6** and **6-^{15}N**, Figure 7, show a similar pattern, but with added coupling to potassium with a 0.44 G coupling constant. These EPR data are consistent with the presence of a $(N_2)^{3-}$ ligand and show no evidence supporting a hydrogen attached to a reduced dinitrogen moiety in the $(N_2H)^{3-}$ alternative.

The experimentally determined structures of **4**, **5**, and **6** were evaluated with density functional calculations using the Tao−Perdew−Staroverov−Scuseria hybrid (TPSSH) functional.[42] The optimized calculated N−N distances of 1.246, 1.380, and 1.387 Å for **4**−**6**, respectively, agree well with the crystallographic data (Table 3).

The DFT results are consistent with an N−N bond order of 2 in **4**. The calculated vibrational frequency of the N−N stretching mode of **4** at 1478 cm^{-1} is close to the experimental value 1425 cm^{-1} determined for **4** by Raman spectroscopy. Raman data were also collected on **4-^{15}N** to confirm the assignment. An absorption at 1377 cm^{-1} was observed that matched exactly the 1377 cm^{-1} value calculated based on the $^{15}N/^{14}N$ mass ratio. In comparison, free diimide, HN=NH, which has a 1.21 Å N−N distance,[56] has an absorption of 1529 cm^{-1},[57] and an absorption at 1622 cm^{-1} has been observed for $\{[C_5H_2(CMe_3)_3]_2Nd\}_2(\mu\text{-}\eta^2\text{:}\eta^2\text{-}N_2)$.[19]

The DFT calculations are consistent with a bond order of 1.5 in **5** and **6**. The DFT results also show a considerable reduction of the calculated N−N stretching frequency value for **5** and **6**. For **6**, the calculated value exactly matches the experimentally determined N−N stretch, 989 cm^{-1}. The experimentally determined stretching frequency 956 cm^{-1} for **6-^{15}N** matches the 955 cm^{-1} value expected based on the $^{15}N/^{14}N$ mass ratio.

Inspection of the computed Kohn−Sham molecular orbitals explains the observed trends in bond lengths and vibrational frequencies. The dinitrogen-Y bonding in **4** results from a strong interaction between an yttrium *d* orbital and the antibonding π^* orbital of N_2 in the YN_2Y plane (Figure 8). The computed natural population analysis (NPA) for N_2 gives a charge of −1.2 and an yttrium *d* population of 0.95 along with the fairly short observed Y−N bond distance of 2.296 Å. This indicates the presence of a polar covalent interaction corresponding to a two-electron four-center bond between two L_2Y fragments and N_2, each with a nearly neutral actual charge. The initial reduction of the N≡N triple bond to a formal N=N double bond in **4** is possible because the occupied *d* orbital of yttrium is high enough in energy and large enough to form a $d_\pi-\pi^*$ back-bond. This is the main basis of the bonding since the occupied bonding σ and π orbitals of N_2 are too low in energy to interact with the metal atoms. The lowest unoccupied molecular orbital of **4** is the essentially unperturbed π^* orbital of N_2 perpendicular to the YN_2Y plane (Figure 8). In **5** and **6**, this orbital is occupied by one unpaired electron. As a result, the N−N bond order drops to 1.5, accompanied by an increase in the bond distance and a decreased vibrational frequency. The unpaired spin density of **5** results almost exclusively from the singly occupied π^* orbital (Figure 9) and is strongly confined to the N_2 ligand. This is in agreement with the EPR data since the 5.8−8.2 G hyperfine coupling constants for nitrogen match those of nitrogen-centered radicals,[56,58,59] whereas the 3.1 G yttrium coupling constant is much less than the 81 G value reported for an yttrium-centered radical.[60]

(56) Doslik, N.; Sixt, T.; Kaim, W. *Angew. Chem., Int. Ed.* **1998**, *37*, 2403–2404.
(57) Bondybey, V. E.; Nibler, J. W. *J. Chem. Phys.* **1975**, *58*, 2125–2134.
(58) Sarkar, B.; Patra, S.; Fiedler, J.; Sunoj, R. B.; Janardanan, D.; Mobin, S. M.; Niemeyer, M.; Lahiri, G. K.; Kaim, W. *Angew. Chem., Int. Ed.* **2005**, *44*, 5655–5658.
(59) Russell, G. A.; Konaka, R.; Strom, E. T.; Danen, W. C.; Chang, K.-Y.; Kaupp, G. *J. Am. Chem. Soc.* **1968**, *90*, 4646–4653.
(60) Zuo, T.; Xu, L.; Beavers, C. M.; Olmstead, M. M.; Fu, W.; Crawford, T. D.; Balch, A. L.; Dorn, H. C. *J. Am. Chem. Soc.* **2008**, *130*, 12992–12997.
(61) Yelamos, C.; Heeg, M. J.; Winter, C. H. *Inorg. Chem.* **1998**, *37*, 3892–3894.
(62) Pfirrmann, S.; Limberg, C.; Herwig, C.; Stößer, R.; Ziemer, B. *Angew. Chem., Int. Ed.* **2009**, *48*, 3357–3361.
(63) Smith, J. M.; Sadique, A. R.; Cundari, T. R.; Rodgers, K. R.; Lukat-Rodgers, G.; Lachicotte, R. J.; Flaschenriem, C. J.; Vela, J.; Holland, P. L. *J. Am. Chem. Soc.* **2006**, *128*, 756–769.

Scheme 2. Reactivity of Dinitrogen with the Yttrium Reduction System, $Y[N(SiMe_3)_2]_3$/Potassium Graphite

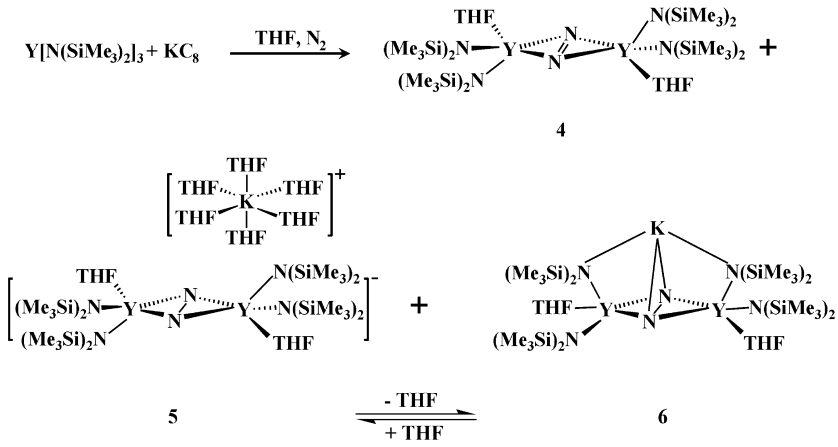

Once the presence of $(N_2)^{3-}$ in **5** and **6** was established, the metrical data could be more fully analyzed. The 2.194(3)−2.247(2) Å Y−N distances in **5** and **6** are significantly shorter than the analogous 2.296(2) and 2.317(2) Å distances in **4**.[23] This is consistent with the more negative charge on the dinitrogen ligand in **5** and **6** vs **4**. The 2.864(2) and 2.885(2) Å K−N distances in **6** are long compared to other K−N distances in the literature. They are near the long end of the 2.763(4)−2.869(4) Å range of K−(η^2-N_2) bond lengths in the potassium pyrazolate complex, [K(3,5-$Ph_2C_3N_2H$)(THF)]$_6$,[61] and they are longer than the 2.714(6)−2.800(6) Å K−(η^2-N_2) distances in K[(β-diketiminate)-Ni]$_2N_2$[62] and K_2[(β-diketiminate)M]$_2N_2$ (M = Fe[63], Ni[62]) complexes in which each potassium has two additional η^6-aryl interactions with substituents on the β-diketiminates. The

Table 3. Calculated and Experimental N−N and Y−N Distances, *d*(N−N) and *d*(Y−N) (Å), and N−N Vibrational Stretching Frequencies, ν(cm^{-1})

compd	*d*(N−N) exp	*d*(N−N) calc	*d*(Y−N) exp	*d*(Y−N) calc	ν(N−N) exp	ν(N−N) calc
4	1.268(3)	1.246	2.296(2)	2.336	1425	1478
			2.317(2)	2.352		
5	1.401(6)	1.380	2.194(3)	2.220	–	1002
			2.218(3)	2.237		
6	1.405(3)	1.387	2.225(2)	2.237	989	989
			2.242(2)	2.265		
			2.231(2)	2.238		
			2.247(2)	2.267		

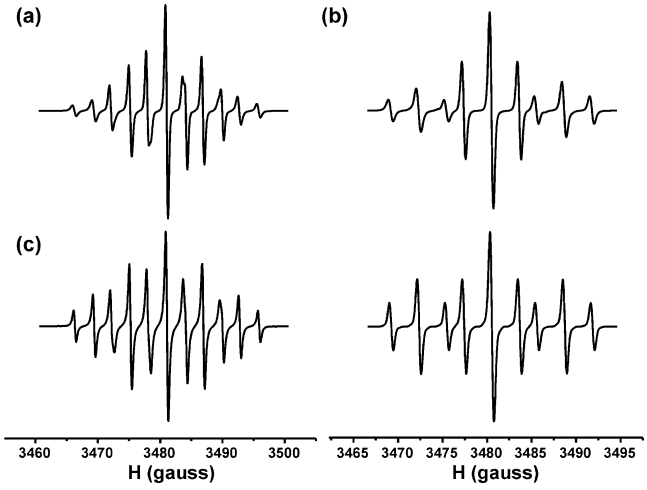

Figure 6. EPR spectra of {[$(Me_3Si)_2N$]$_2$(THF)Y}$_2$(μ-η^2:η^2-N_2)[K(THF)$_6$], **5**: (a) **5** at 293 K in millimolar THF solution, (b) **5**-^{15}**N** at 293 K in millimolar THF solution, and (c) the simulated spectra.

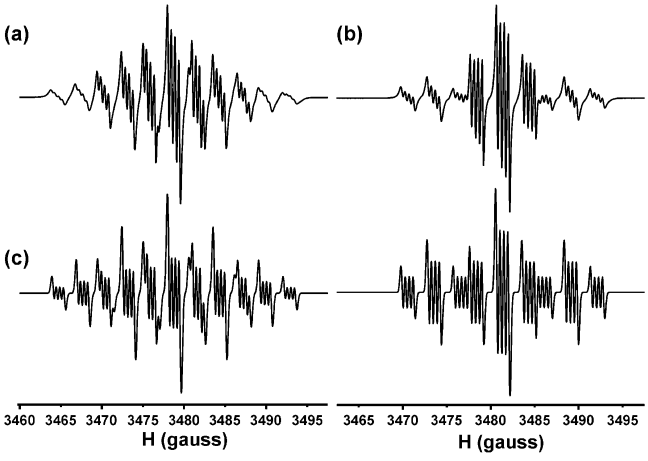

Figure 7. EPR spectra of {[$(Me_3Si)_2N$]$_2$(THF)Y}$_2$(μ_3-η^2:η^2:η^2-N_2)K, **6**: (a) **6** at 293 K in millimolar toluene solution, (b) **6**-^{15}**N** at 293 K in millimolar toluene solution, and (c) the simulated spectra.

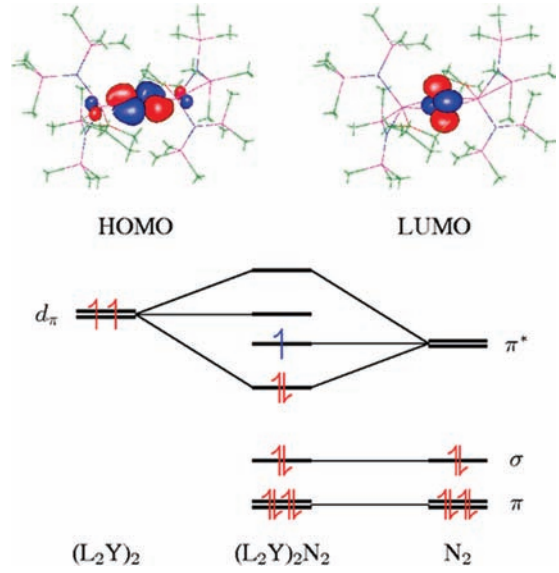

Figure 8. Simplified molecular orbital scheme of **4** with eight electrons shown in red. The highest occupied molecular orbital (HOMO) shows a two-electron four-center Y(d_π)−N(π^*) bond, while the lowest unoccupied molecular orbital (LUMO) is an essentially unperturbed dinitrogen π^* orbital. In **5** and **6**, this LUMO is occupied by one unpaired electron, depicted in blue.

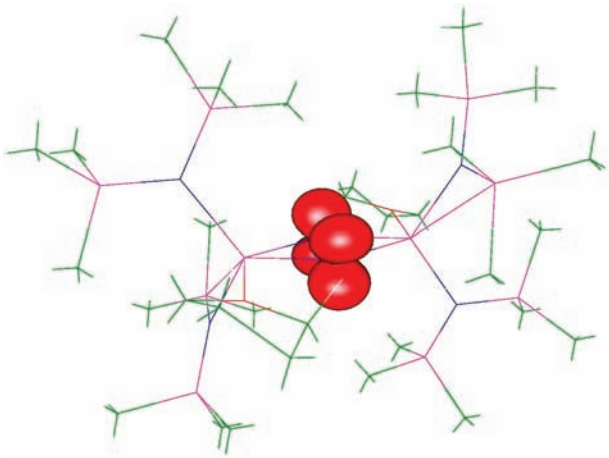

Figure 9. Computed spin density of $\{[(Me_3Si)_2N]_2(THF)Y\}_2(\mu\text{-}\eta^2\text{:}\eta^2\text{-}N_2)[K(THF)_6]$, **5**.

long distances are consistent with the small potassium coupling constant.

Conclusions

These results show that, under the appropriate conditions, $(N_2)^{3-}$ is a viable reduction product of dinitrogen. It is possible that, in transition metal systems with more orbital interactions, complexes of this radical have too fleeting an existence to be detected. The DFT calculations show that the unpaired electron is isolated in an orbital perpendicular to the metal orbitals and protected from the external environment by the other ligands on the metals. Since biological systems often can provide unusual protective coordination environments via tertiary structure, all viable intermediates on the nitrogen to ammonia pathway should be considered in the search for chemical mimics of biological systems.

Acknowledgment. We thank the U.S. National Science Foundation for support of this research (CHE 0703372, 0723168 and 0809384), the Swiss National Science Foundation for a postdoctoral fellowship for G.Z., and D. C. Lacy, Drs. E. Fadeev, and A. J. DiBilio, as well as Professors M. J. Nilges, R. D. Britt, and A. S. Borovik for help with EPR spectral studies.

Supporting Information Available: X-ray crystallographic files for **1**, **2**, **3**, **5**, and **6**. This material is available free of charge via the Internet at http://pubs.acs.org.

JA9036753